Chapter 18

Viewing sub-surface for an effective managed aquifer recharge from a geophysical perspective

Shakeel Ahmed, Tanvi Arora, Sarah Sarah, Farooq Ahmad Dar, Tarun Kumar Gaur, Taufique Warsi and Pasupunoori Raghuvendar

18.1 INTRODUCTION

Managed Aquifer Recharge (MAR) is a technique of intentional storage and treatment of water in aquifers where natural recharge processes have been affected (Dillon, 2005; Dillon *et al.*, 2009). MAR is a cost-effective process that has solved groundwater quantity and quality problems in many of the world's stressed aquifer systems (Gale & Dillon, 2005).

Natural processes of groundwater recharge have been highly influenced and affected by climate change, urbanization and other unmanaged anthropogenic practices. Groundwater is drafted at a rate which cannot be replenished through natural recharge conditions alone. Groundwater quality is constantly deteriorating due to uncontrolled dumping of waste directly in groundwater interacting zones. Therefore, artificial recharge and MAR is of great interest to replenish the heavy losses of groundwater for sustainable management of the aquifers by enhancing natural infiltration and recharge processes through purposeful and managed activities (Dillon *et al.*, 2009).

The process of aquifer recharge involves and is influenced by both surface as well as sub-surface characteristics. However, in the estimation and evaluation of aquifer recharge, often only surface features and not the sub-surface features are considered, as the latter are much more complex and hidden compared to the surface features that are visible and easily mapped. The sub-surface contains both unsaturated and saturated zones and the two have very contrasting properties. Thus, to investigate the sub-surface, geophysical methods are promising tools as they are mostly non-invasive and reveal the physical properties of the sub-surface. In this chapter relevant geophysical techniques applicable for MAR investigations and their application are briefly described.

18.2 UNIQUE CONTRIBUTIONS AND CHALLENGES OF HYDRO-GEOPHYSICS

Geophysical methods are merely based on the physical properties of sub-surfaces. Hydro-geophysics is an evolving but useful field for understanding aquifer systems, their geometry, the extents and characteristics. Due to non-uniformity in such systems, it is important to identify a suitable geophysical method to develop an approach for identifying water-bearing structures or specific points of recharge to aquifers. Audio Frequency telluric methods (AFTM) have been used to detect water in karst settings (Chen, 1988; CGS, 2005; Gan *et al.*, 2011) and also in combination with induced polarization to identify existing fissures (Li & Wang, 2009). Time domain electromagnetic is of limited use in carbonate terrenes (Chalikakis, 2006; Ezersky *et al.*, 2006). Very low frequency (VLF) methods have helped detect epikarst and also locate near surface heterogeneities, but with a limited resolution (Turberg & Barker, 1996; Bosch & Müller, 2001, 2005). Integrated with electrical resistivity tomography (ERT), VLF provides good results to map productive aquifers for precise location of wells (Alexopoulos *et al.*, 2011; Vargemezis *et al.*, 2011). Other methods like gravimetry (based on density variations), magnetic resonance sounding

(to locate water content), mise-à-la-masse (to trace water filled cavities), self-potential (to map preferential pathways) are employed with specific success (Jacob *et al*., 2009; Guérin *et al*., 2009; Jardani *et al*., 2006; Meyerhoff *et al*., 2012). Very few studies focused on the use of geophysical microgravimetric and gravity gradient techniques to target sub-surface cavities and karst features (Colley, 1963; Neumann, 1965; Butler, 1984; Blizkovsky, 1979). Kaspar and Pecen (1975) used an electromagnetic (EM) method for tracing karst features in eastern Slovakia by means of differences in electrical properties between limestone and karst features. Moore and Stewart (1983) used seismic refraction, ERT and microgravity to delineate zones of increased fracture density.

In the past decade Electrical sounding and Resistivity tomography (VES & ERT) have evolved, potential geophysical technologies to monitor the natural changes in shallow sub-surface resistivity (Binley *et al*., 2002; Dutta *et al*., 2006, Arora & Ahmed, 2010, 2011; Loke *et al*., 2014; Singha *et al*., 2014). ERT can be applied to define the water table (Zaidi, 2012), to delineate aquifers (Dutta *et al*., 2006), to search for karst geological structures (Leuccim, 2005) and find karst water (Metwaly *et al*., 2012; Vlahović & Munda, 2011; Gan *et al*., 2013) and also to study the unsaturated zone (Arora, 2013; Carriere *et al*., 2013).

We present three case studies: one from the Chandi limestone of Raipur city, a second from a dugwell site in crystalline aquifers and a percolation tank in granitic terrene of Maheshwaram watershed, all of which are poorly understood in terms of hydrogeology which demands detailed research before taking any MAR program in the area. The purpose of MAR in these areas is to infiltrate excess surface run-off to the aquifer for a smooth supply and demand of groundwater for future uses. The implementation of MAR and its success depend highly on the knowledge of the hydrogeological setup of the aquifer.

The purpose of this chapter is to demonstrate, how conceptual models of the three aquifers are developed through hydro-geophysical approaches. The results will help locate the best suitable sites for implementing artificial recharge schemes and to assess their feasibility. This work will have great impact on the operation, management, maintenance and expansion of MAR in areas which are still little understood in the Indian context.

18.3 GEOPHYSICAL METHODS

18.3.1 Hydro-geophysical electrical methods

The relationship between electrical resistivity, current and the electrical potential is governed by Ohm's law. The Poisson's equation is used to calculate the potential in a continuous medium, the form of Ohm's Law, combined with the conservation of current. Loke (2013) defined the potential due to a point current source located at x is given by

$$\nabla\left[\frac{1}{\rho(x,y,z)}\right]\nabla\phi(x,y,z) = \frac{\partial j}{\partial t}\delta(xs) \tag{18.1}$$

where ρ is the resistivity, ϕ is the potential and j is the charge density.

Knowledge of the resistivity distribution can aid in calculating the potential at any point either on surface or in the medium. Here, the purpose of the resistivity method is to calculate the unknown distribution of electrical resistivity in the sub-surface. The measurements for the resistivity survey are made by passing a current into the ground through two current electrodes (usually metal rods), and measuring the difference between the voltage at two potential electrodes. Basically, the resistivity meter has a current source and voltage measuring circuitry that are connected by cables to the electrodes (Figure 18.1).

There exist different configurations as drawn in Figure 18.1. Many workers like Dahlin and Zhow (2004), Saydam and Duckworth (1978), Szalai and Szarka (2008) and Zhou *et al*. (2002) have clearly discussed the pro's and con's of various configurations. We need to accept and adopt a particular configuration depending on the need of the interest of the field objective. The multi-channel system utilises the multiple gradient configuration (shown above) and was specially described by Loke *et al*. (2013) and Dahlin and Zhou (2004).

We consider that potential difference is directly proportional to the current injected. By assuming a constant, called geometrical factor (k), we calculate the apparent resistivity (ρa) value by the formula given in equation (18.2).

$$\rho a = k\frac{\Delta V}{I} \tag{18.2}$$

k is the geometric factor which depends upon the array configuration adopted in field (Koefoed, 1979).

The equation (18.2) represents the inverse problem with the assumption of homogenous and isotropic sub-surface to carry out resistivity measurements.

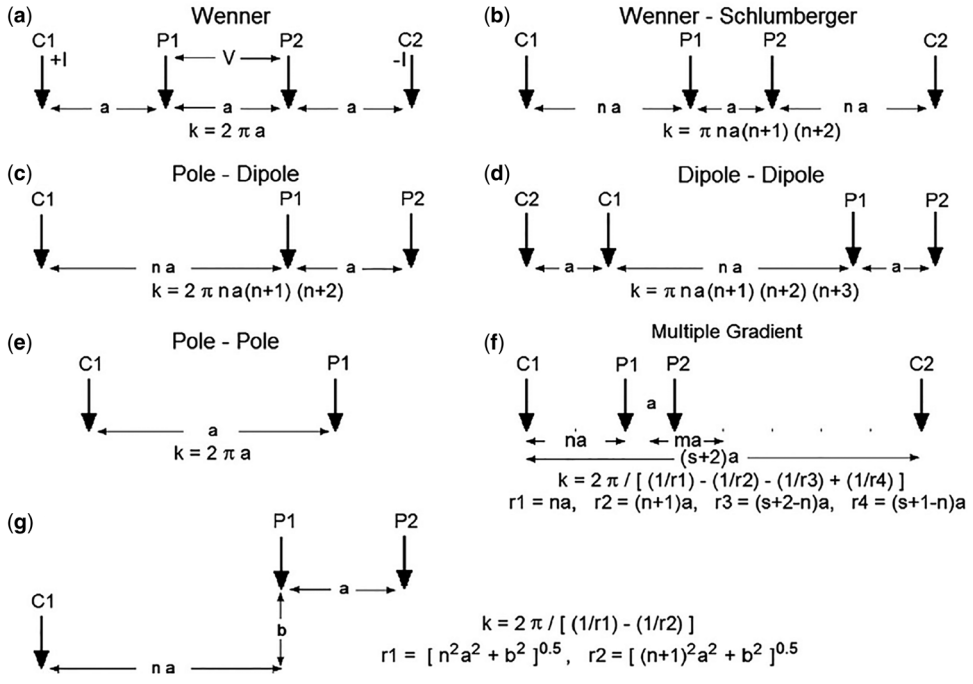

Figure 18.1 Some commonly used electrode arrays and their geometric factors. Note that for the multiple gradient array, the total array length is '(s + 2)a' and the distance between the centre of the potential dipole pair P1–P2 and the centre of the current pair C1–C2 is given by 'ma'. British Geological Survey National Environmental Research Council 2013 (modified after Loke *et al.*, 2014).

Let us consider the Schlumberger configuration (Figure 18.2). The distance between AB is 2s and between MN is 2b.

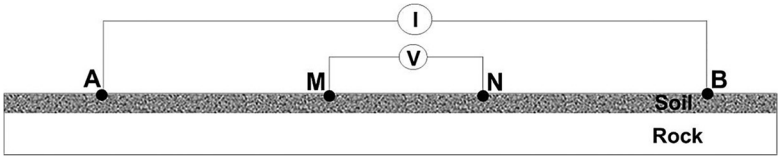

Figure 18.2 An electrode layout for the Schlumberger configuration.

The current I is flowing between AB, the potential at M due to current electrodes A and B is given by:

$$V_M = \frac{\rho_a I}{2\pi}\left[\frac{1}{\mathrm{AM}} - \frac{1}{\mathrm{MB}}\right] \tag{18.3}$$

when ρ_a is known as apparent resistivity.

Similarly, the potential at N due to current electrodes A and B is:

$$V_N = \frac{\rho_a \mathrm{I}}{2\pi}\left[\frac{1}{\mathrm{AN}} - \frac{1}{\mathrm{NB}}\right] \tag{18.4}$$

The potential difference will be

$$\Delta V = V_M - V_N \tag{18.5}$$

$$\Delta V = \frac{\rho_a I}{2\pi}\left[\frac{1}{\mathrm{AM}} - \frac{1}{\mathrm{MB}} - \frac{1}{\mathrm{AN}} + \frac{1}{\mathrm{NB}}\right] \tag{18.6}$$

After writing AM, MB, AN and NB in terms of *s* and *b*, the expression of apparent resistivity will be given by:

$$\rho_a = \frac{\pi(s^2 - b^2)}{2b} * \frac{\Delta V}{I} \tag{18.7}$$

Here $\frac{\pi(s^2 - b^2)}{2b}$ is known as geometrical factor for the Schlumberger configuration.

Vertical electrical soundings (VES)

Electrical resistivity surveys have been used for many decades in hydrogeological, mining and geotechnical investigations. The direct-current electrical resistivity method for conducting a vertical electrical sounding (VES) has proved very popular in groundwater studies due to the simplicity of the technique and the ruggedness of the instrumentation. There are a number of configurations available for electrical surveys of which either the Schlumberger or Wenner configuration are most useful for sounding, since all commonly available interpretation methods and interpretation aids for sounding are based on these two configurations. When using either method, the centre point of the configuration should be at a fixed location, while the electrode location varies around it. The apparent resistivity values and layer depths interpreted from them are referred to the centre point.

Multi-electrode systems and 2-D imaging surveys

The typical sounding and profiling resistivity methods makes use of four electrodes connected to four individual cables. On the one hand, these methods provide only 1-D section of the medium, the use of multi-electrode systems help in capturing 2-D vertical as well as horizontal pictures of the medium. Normally there are more than 24 electrodes connected through a multi-core cable (Figure 18.3). The current and potential electrodes are maintained at regular fixed interval from each other and are progressively moved in a line on the ground. At each step, one set of measurement is recorded. The set of all measurements at the first electrode gives a profile of resistivity values. Then the electrode spacing is increased further and second set of measurements are completed. This process of increasing spacing (by a factor of n = 2) is repeated until the maximum spacing between the electrodes is reached. It should be taken into consideration that the depth of investigation depends on the large values of "n".

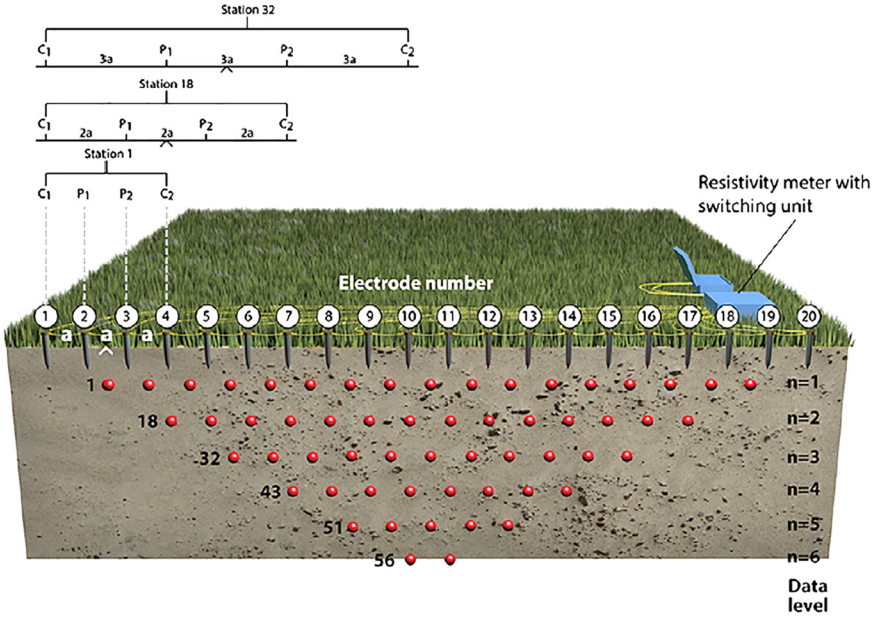

Figure 18.3 Schematic diagram of a multi-electrode system, and a possible sequence of measurements to create a 2-D pseudosection. British Geological Survey, National Environmental Research Council 2013 (modified after Loke *et al.*, 2014).

As suggested by Loke and Barker (1996a), there should be large number of rectangular cells in the 2-D section to infer the maximum information out of it. There are both horizontal and vertical variations in the resistivity values of the cells. Inversion

of these measured resistivities is very important before interpretation because the raw resistivity measurements rarely give the true section of the surface.

In the presented study resistivity measurements were carried out with the resistivity meter Syscal R1 Junior (IRIS Instruments, Orléans, France) equipped with 48 electrodes in different spacing (4, 6 and 10 m depending on spatial constraints) and ABEM Terrameter equipped with 120 electrodes with various spacing. The intensity and voltage accuracy is 0.3%, which is consistent with the measurements carried out under constant hydro-geologic conditions for about ten hours persistent within a tenth of an ohm-meter, i.e. one thousandth of the measured resistivity could reach several ohm-meters between two sets of measurements 1 hour apart. Inversion was made with the RES2DINV software (Loke & Barker, 1996a). This technique, based on the smoothness-constrained least squares method, produced a 2-D sub-surface model of the resistivity section.

18.3.2 Time domain electromagnetic methods (TDEM)

Time Domain Electromagnetic Methods (TDEM) are also primarily used for resistivity sounding. TDEM measurements are carried out by sending an electrical current through a transmitter coil. When the transmitter current is shut off, induction creates a decaying primary magnetic field, which in turn induces secondary electric currents (that are essentially a shallow "image" of the former transmitter current) with their accompanying magnetic fields. The decay of the induced field over time (which depends on the electric properties of the ground) is monitored with a separate receiver coil. TDEM provides a wide range of effective sounding depths from approximately 6 to 900 meters. In karst hydrogeology, TDEM is useful for determining the depth and thickness of overburden, depth of the water table, depth and degree of saltwater (or ion-contaminated water) intrusion, and detection of fracture zones (e.g. Farrell *et al.*, 2003). TDEM provides good lateral as well as vertical resolution, and a wide range of effective survey depths. The method is sometimes limited by the requirement for impractically large (e.g. 300×300 m or larger) transmitter coils to achieve deep measurements. Though we adopted this technique in the Karst terrene the results of TDEM are not consistent with the ERT due to conductivity variations.

18.3.3 Borehole resistivity logging

Well logging, also known as borehole logging, is the practice of making a detailed record (a well log) of the geologic formations penetrated by a borehole. The log may be based either on visual inspection of samples brought to the surface (geological logs) or on physical measurements made by instruments lowered into the hole (geophysical logs). Resistivity logging is a method of well logging that works by characterizing the rock or sediment in a borehole by measuring its electrical resistivity.

This survey presented in this study was done to identify the contact zone between the weathered layer and the bedrock. It is also useful to investigate the zones supplying water to the wells. This is based on the principle of Ohm's law and is used to calculate the resistivity of the sub-surface formation. There are several electrode configuration methods like one-electrode, two-electrode (short normal, long normal) three-electrode methods etc. In the present case, a resistivity probe with two electrodes was used, which was fabricated at IFCGR, NGRI (Figure 18.4).

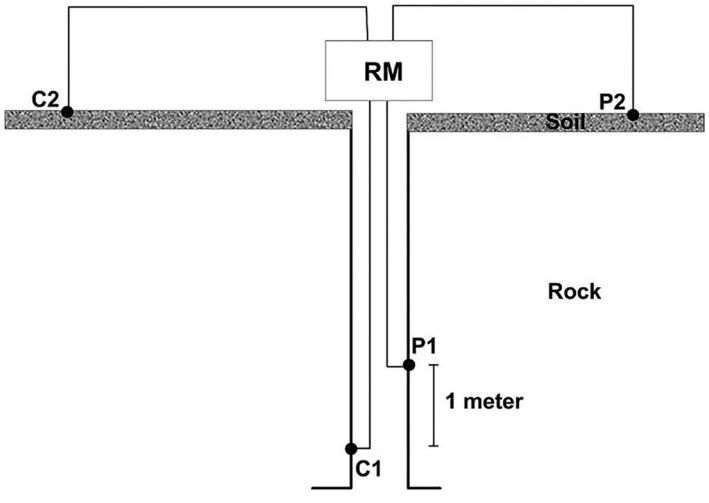

Figure 18.4 Logging circuit diagram of the geophysical borehole logger fabricated at IFCGR, NGRI.

The probe consists of two electrodes: one is used as current electrode and the second is used as potential electrode and the spacing between the two electrodes is 1m. The other two (current and potential) electrodes are kept far away from the bore hole. The probe is then lowered into the bore hole and every 0.5 m the measurement is recorded till the bottom of the well. The instrument used for this technique was "SYSCAL switch (Junior)" which measures current and potential. The resistivity values were plotted against corresponding depths which gave the resistivity log of the particular bore well. Boundaries of formations having different resistivities are detected most readily with short electrode spacing; whereas information on fluids in thick permeable formations can be best obtained with long spacing.

18.4 CASE STUDIES PERTAINING TO MAR

18.4.1 Finding conducting zones in Karst aquifer systems and analysing the efficacy of proposed recharge structure

The study area was Raipur, an example for a water stressed city where urbanization poses a threat by altering the hydrological scenarios. This work highlights possibilities for assessing the efficiency of MAR by using hydro-geophysical techniques to study the structure of the unsaturated zone of karst terrene of Central India, where soil cover is very thin and followed by shale formation that are not suitable for recharge.

Electrical resistivity sounding was carried out at 12 sites to detect conductive zones along the local surface drainage in the area. The Chokhra nalah is the main local drainage along which MAR structures need to be proposed in the Telibandha area of Raipur (Figure 18.5). We did close soundings from VES method thereby capturing the local resistivity variation in the area. After the dense VES, ERT with 4–10 m spacing using Wenner-Schlumberger and gradient methods was carried out.

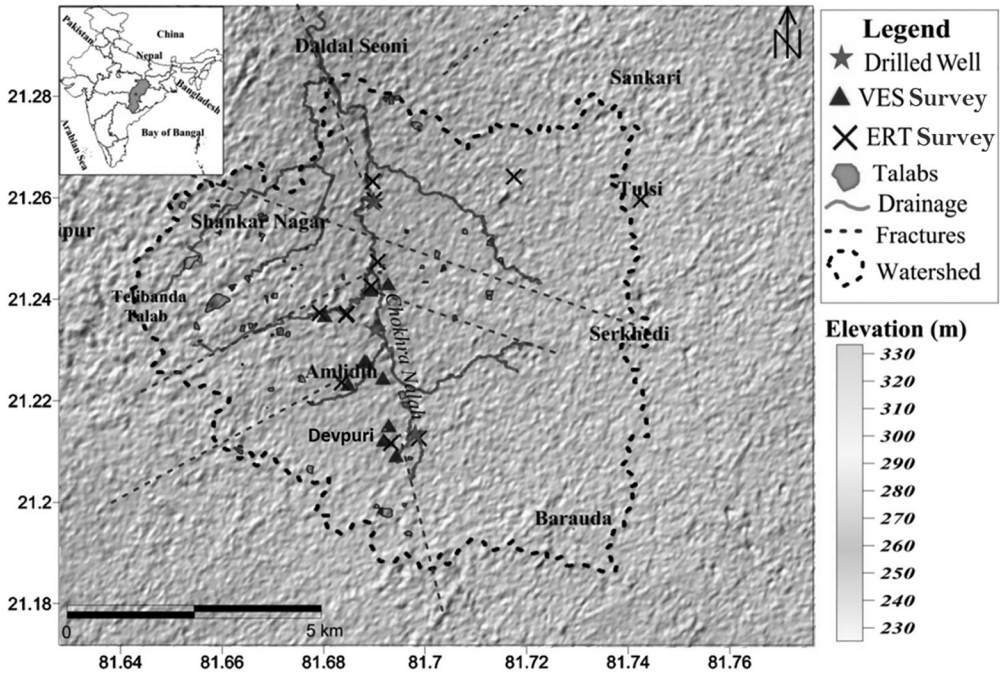

Figure 18.5 Digital Elevation map of the Telibandha area at the outskirts of Raipur city. The map also shows the location of various measurement points.

Digital elevation model (DEM)

A Digital Elevation Model (DEM) from ASTER (Advanced Spaceborne Thermal Emission and Reflection Radiometer) of 30×30 m resolution was used for topographic interpretation. Watershed and drainage were delineated using the Spatial Analysis Toolbox of ArcGIS software. The lineaments were digitized from the shaded relief maps of DEM with different sun angle (Figure 18.5).

Vertical electrical sounding (VES)

Figure 18.6 shows the resistivity values for layers at different depths interpreted by using the 1X-1D software (www.interprix.com). The resistivity values range from as low as 5–200 ohm m to as high as 2,000–3,000 ohm m.

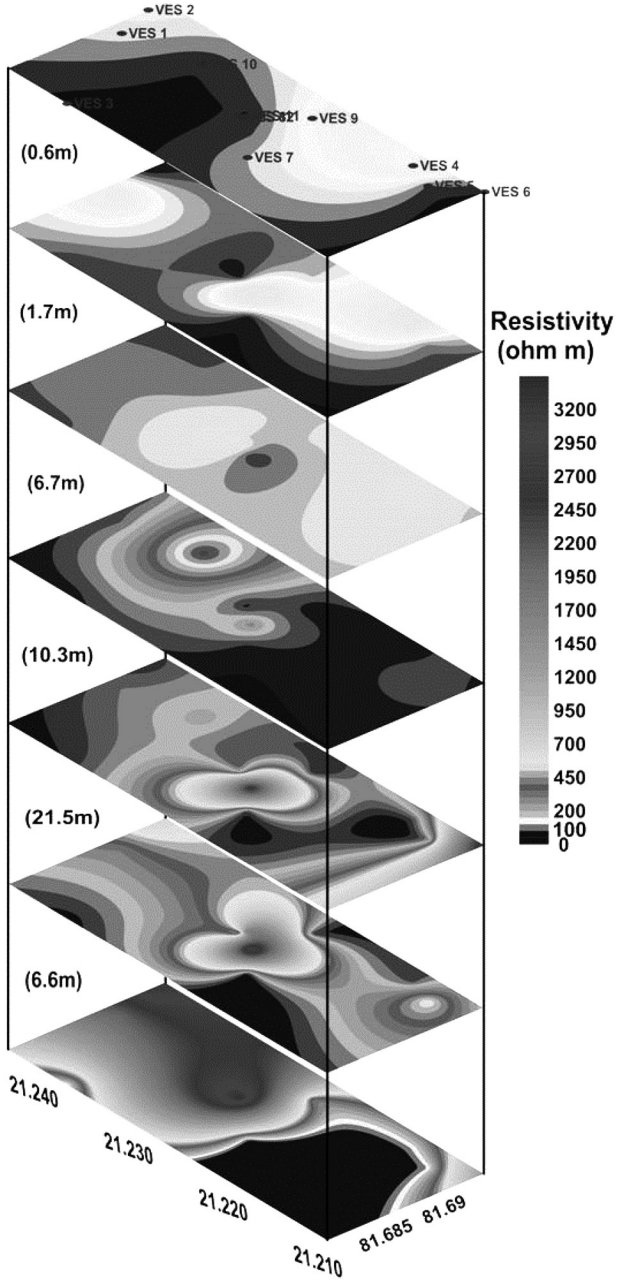

Figure 18.6 Results of Vertical Electrical Sounding (VES) at different depths. The black dots are the location points of the VES as shown in Figure 18.5.

The profiles show a sharp transition zone at the depth of 2.3 m (layer 3). As we interpret the deeper layers, the high resistivity value concentrates towards point VES 8 (at the centre). This shift gives an indication of an existing paleochannel between points VES8 and VES10or some weak structure, as it would be typical for a karst aquifer system. Accordingly, the area around VES 8 may be a suitable site for recharge.

Electrical resistivity tomography (ERT)

Electrical Resistivity Tomography (ERT) was carried out along 12 selected areas in and around Telibandha area. Exemplarily, the results for Station Devpuri (Figure 18.5) are given. The profile was laid down in NW-SE direction along 480 m with electrode spacing of 10 m. The Wenner-Schlumberger configuration was used to survey the profile. A total number of 529 datum points were measured at 23 data levels, allowing to plot a pseudo cross-section (Figure 18.7). The results clearly show the layered structure of the limestone in the sub-surface. Resistivity varied with the water content showing a thick layer of 15–20 m thickness of damp limestone with resistivity varying between 50–150 ohm m at a depth of 5 m and up to 90 m with high resistivity of more than 300 ohm m of dry limestone below.

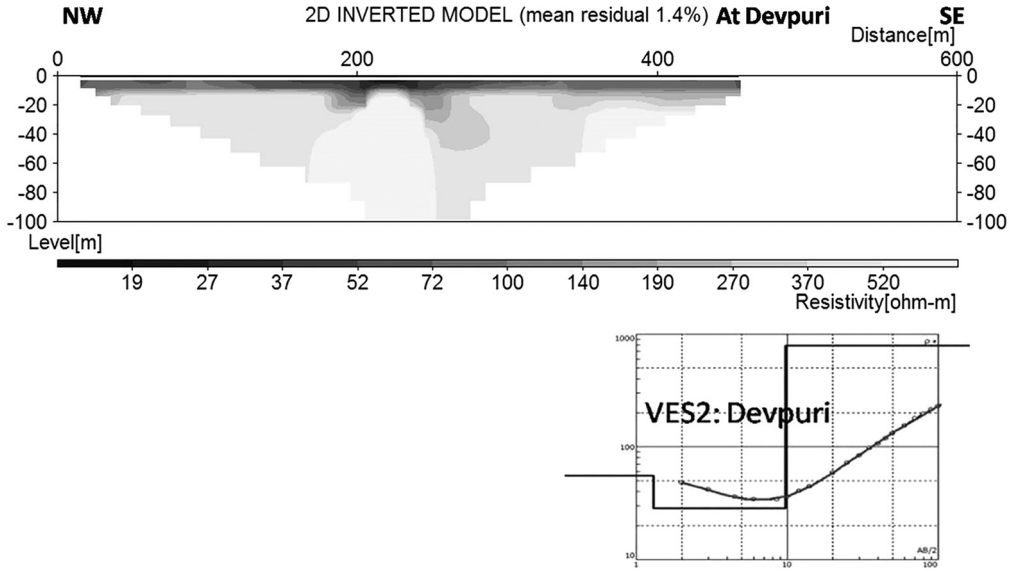

Figure 18.7 Electrical Resistivity Tomogram at station Devpuri.

The area of interest remains limited to 35–40 m below the surface, however many strong lateral and vertical anomalies were found in the ERT surveys. The low resistivity in the unsaturated zone, as compared to the high resistivity of limestone bedrock, is the target for preferred pathways. The low resistivity anomalies in the 2D inverted sections could be water-filled conduits or solution channels. These were later confirmed with the lithology of drilled wells at 3 sites. The borehole logging results correlated very well with the resistivity of ERT survey and lithology. Lithological information confirmed that the solution activity has modified the hydraulic properties of the aquifer by widening fractures, bedding planes and developing solution voids. Local heterogeneity was mapped based on the resistivity variations thereby proposing the favourable sites for construction of MAR structures. Along with it the surface implications of the hiding mafic dykes were inferred in the area.

After the complete detailed investigations, a combined map showing the conductive and resistive zones was generated (Figure 18.8). Then sites for 3 borewells were proposed and drilled to correlate the hydro-geophysical parameters to the lithology. The lithological data of three bore holes gave a clear understanding of the sub-surface geology of the limestone aquifer. The aquifer is overlain by a top black soil layer of 1–6 m thickness which possesses a high clay content, nodules (kanker) and is rich in iron matter. Below this layer flaggy limestone with a high clay content occurs down to the fresh limestone. This indicates that the weathered zone overlying the limestone is generally of ~6 m depth. Below this zone fresh limestone is encountered where two fracture zones and solution activity is observed mostly in the central part of the watershed. The solution channels are filled with sediments/soils and indicate their collapsed nature which can also be related to the presence of solution type features on the surface and presence of more surface ponds/talabs. The fresh black limestone up to about 40m depth has two fracture zones with high groundwater yield and little solution activity indicating the effect of karstification processes in the limestone. The solution weathering in other layers was found to be insignificant. The results were used to analyse the secondary porosity at a particular site to assess the quantity pore spaces available for recharging and storing water.

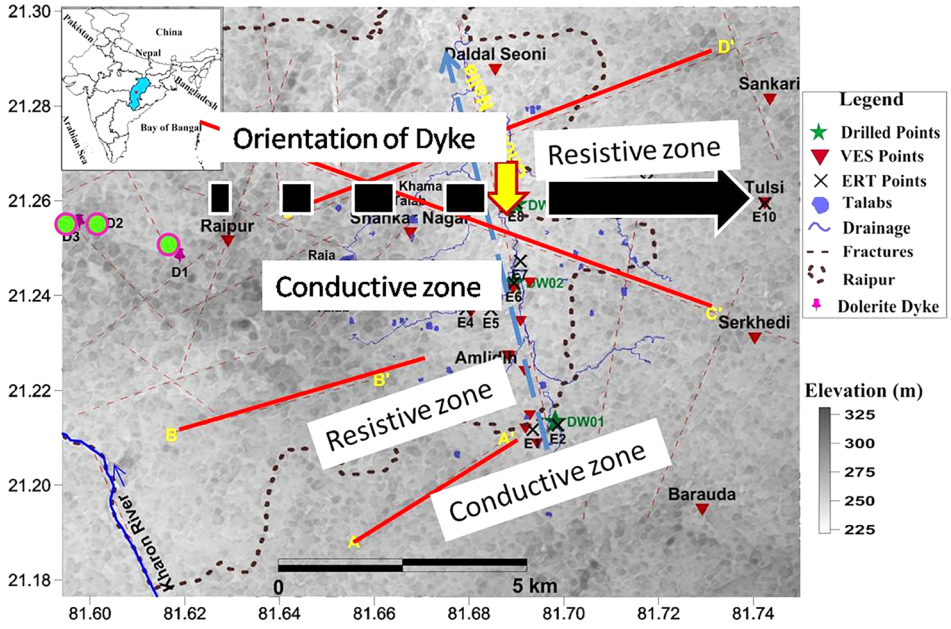

Figure 18.8 Results of Surface Electrical Structure mapping of the area suggesting the favourable zones for MAR. Black arrow indicates the possible trace of hidden sub-surface dyke. Black lines are drawn to demarcate the resistive and conductive zones on the surface based on resistivity data.

18.4.2 Recharge through intervention in dugwells in a crystalline aquifer: Assessment using time lapse electrical resistivity tomography (TLERT)

Natural recharge due to infiltration is variable and also influences the correlation between the structures deducted from geophysical data with respect to time. This spatial variation of the electrical resistivity has been documented in this study by the tomogram analysis of 2D electrical resistivity imaging data. The tomograms added precision to the analysis of the moisture movement, as it is more accurate and rigorous at spatial imaging of electrical resistivity data.

The long duration imaging surveys with a frequency of 14 days were carried out by Arora & Ahmed (2011) at a site along the profile with a length 96 m with electrode spacing of 2 m. The unsaturated zone had been mapped up to a depth of 12 meters. These tomograms of the data acquired between 15th October 2004 (post monsoon of 2004) and 15th October 2005 (during the monsoon period of 2005) at one of the sites were re-analysed and re-interpreted as a part of the project work as shown in corresponding Figure 18.9.

The resistivity data were processed and interpreted with the help of RES2DINV software developed by Loke and Barker (1996a) following an iterative optimization approach. The resulting tomograms of the data acquired between 15th October 2004 (post monsoon of 2004) and 15th October 2005 (during the monsoon period of 2005) at site S1 were further analysed in regards to soil water content in the scope of this study and interpreted with regard to the movement of the water infiltration front. Figure 18.9 shows the tomograms of the time period 12th July 2005 to 11th September 2005. Thereby, low electrical resistivity corresponds to increased soil water content and the subsequent plots (A to L) show the change in resistivity from one time-step to another. The observed changes indicated both, a vertical and horizontal movement of infiltrating water.

Published TLERT data from Arora & Ahmed (2011) for the monsoon cycle of 2005 were taken and further improved for analysis. In this study we concentrated on the resective zones where the recharge could possibly take place. Quantitatively the percent differences in electrical resistivities associated with the arrival of the recharge match the recharge measurement fairly well, both in time and space. Between 20 m and 42 m along Zone 1 (Figure 18.9), a non-uniform distribution of moisture in the vertical profile following the infiltration after a rainfall event indicates a zone of preferential natural recharge. Between 68 m and 76 m along profile the Zone 3, the variation in resistivity is most presumably due to different geological materials exhibiting different porosities.

After the time lapse experiment and observing the water level fluctuations in one of the monitoring dug wells, it was recommended to construct rain gardens (large recharge pits with plants) in the surrounding areas. In total, three rain gardens were constructed up to a depth of 1.2 m from the surface enabling maximum recharge to the aquifer. A positive effect of the

recharge was observed in all the bore wells and dug wells within the study area as evident from 0.5m to 1.0 m additional rise in groundwater levels.

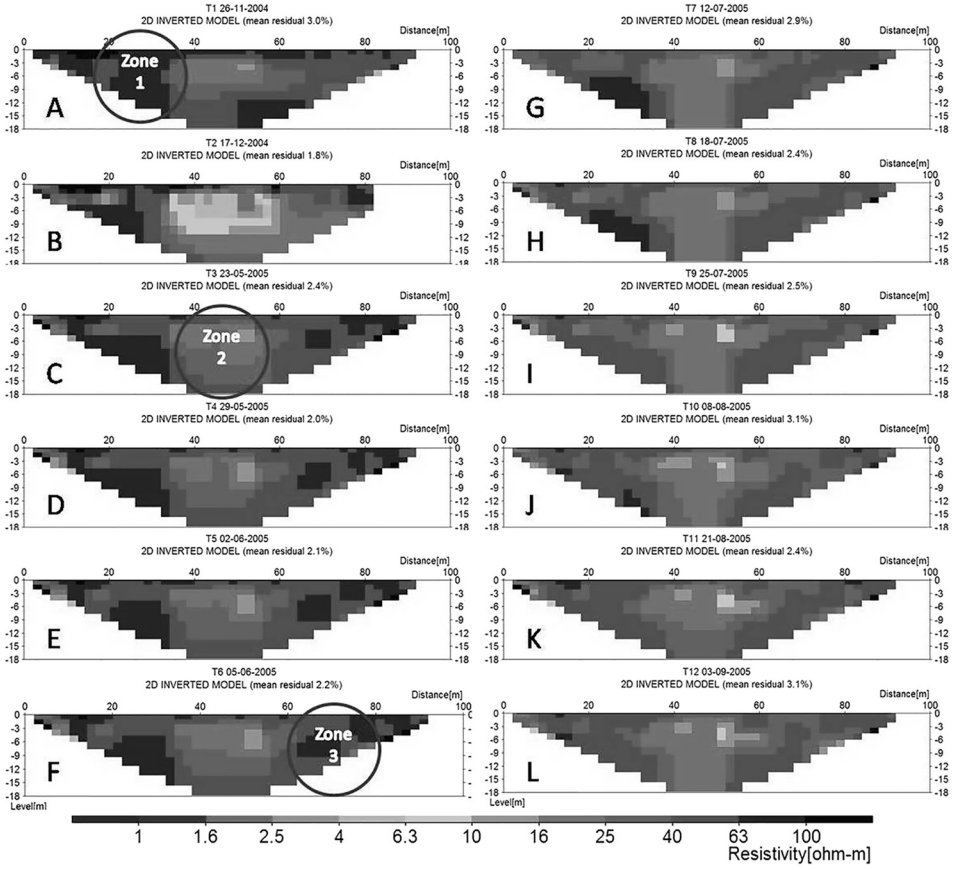

Figure 18.9 Inverted resistivity models for the time-lapse experiment carried out in the study area for the monsoon cycle of 2005 (labelled from A–L) (modified after Arora and Ahmed, 2011).

18.4.3 Infiltration in a percolation tank and effectiveness of check dams

Geophysical investigations around a percolation tank

The investigated area was the Tumulur percolation tank located in the north-eastern part of the Maheshwaram watershed, which is underlain by weathered Archaen biotite granite. Its weathering profile leads to a stratified aquifer with two distinct layers (Dewandel *et al.*, 2006): The saprolite (10–15 m thick layer from the surface) is characterized by sandy-clay material. Its total porosity is relatively high (up to 10%), but due to the clay content the effective porosity is low. In total five ERT profiles were acquired in different orientations to investigate the tank in and around area. The same methodology of ERT was undertaken (as mentioned in above sections) using the IRIS instrument Syscal Junior with 48 electrodes. The variable electrode spacing from 4–10 m was used for different profiles. After the data acquisition, the raw resistivity data was inverted and modelled to acquire the pseudo section using the RES2DINV software by Loke and Barker (1996a).

The ERT profile A (Figure 18.10) shows an increase of the saprolite layer thickness from west to east, at a depth of 10–25 m. In the profile B, the saprolite thickness trends around 10–15 m all through the N–S profile. But the fractured media is encountered towards the south of the profile, intersecting the profile A. Towards the northern end, there is basement rock dipping in N–S direction. While considering the profile C, there is a homogeneous saprolitic layer all through the NE-SW trending profile, but the fresh basement is quite shallow. This B and C profiles intersects at a point and confirms the results sections obtained individually. The information obtained is in agreement with the observations of the bore cutting (Boisson *et al.*, 2014). These profiles were used to complement previous data obtained on watershed scale to produce maps of saprolite thickness and alternated zone thickness (Boisson *et al.*, 2014) on tank scale. ERT data was integrated to the previous datasets through interpolation using the kriging method.

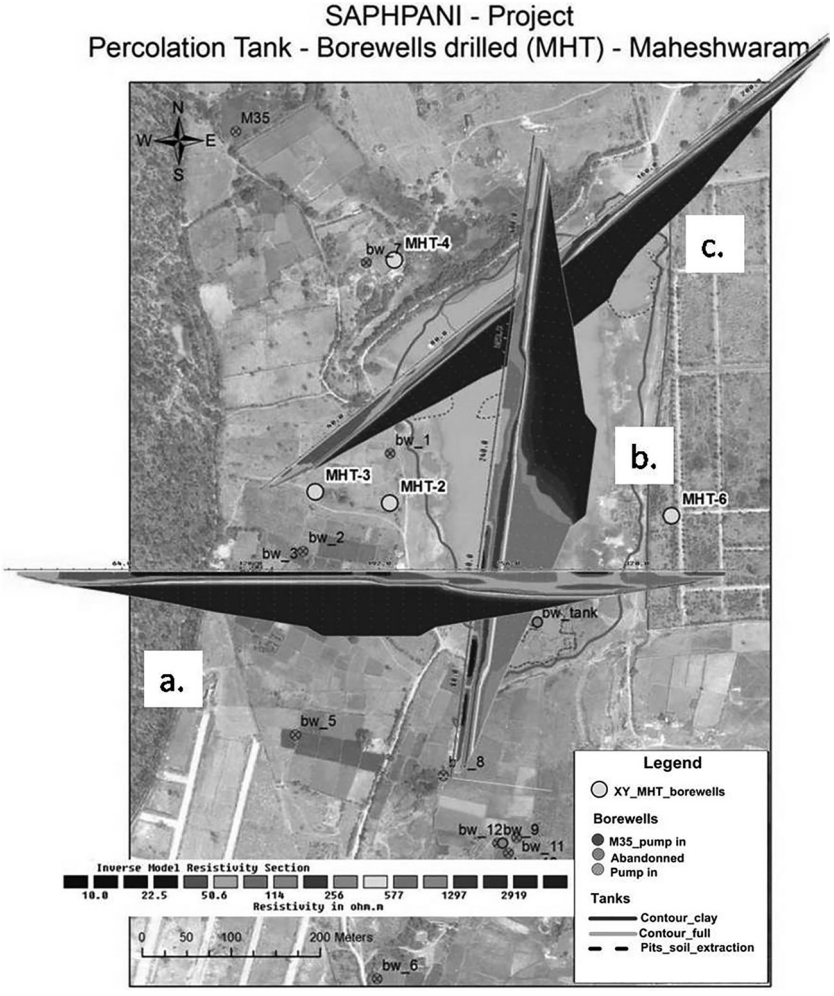

Figure 18.10 ERT profiles carried out around the percolation tank in different orientations. A total 5 profiles were taken, of which 3 are shown here.

Verification of artificial recharge effectiveness through simulation studies

The numerical model of aquifer flow in the area of Maheshwaram, including the simulation of tank recharge, was available in the same project (Chapter 14). It was therefore, useful to study and validate a new scenario for the Artificial Recharge through the tank at a favourable point provided by the geophysical investigations.

The effect of the Tumlur tank, with an area of 0.14 km^2, was initially simulated in steady state and then in transient condition within the regional model. The tank area was divided into meshes of 50 m by 50 m, giving about 57 active meshes for micro scale modelling. The steady state simulation had been performed for averaged rainfall and abstraction values in and around Tumlur tank for the period January 2001 and was then calibrated under transient conditions for the periods 2001 to 2006. This model was calibrated against the general recharge and hydraulic conductivity.

The meshes in the tank area (Figure 18.11) were divided into two parts through a hypothetical barrier, simulating a check-dam. Thus extra recharge (additional as Artificial Recharge) was assigned once to the northern side of the check dam as if the check dam was absent, simulating the logging of water under natural condition and on another run, the same extra recharge were assigned to the meshes at the southern side of the check dam only as the proposed check dam would not have allowed water to flow to the lowest point. The model was run in both conditions for a period of 6 years keeping all other inputs the same. The respective rises in groundwater levels at a representative observation point in both the cases were plotted for 6 years or 12 seasons (Figure 18.12b). It could clearly be seen that if the run-off water is applied to the southern portion of the tank, by creating an engineered structure, the benefit to the system will be manifold. To determine the exact location of such a check dam geophysical investigations are recommended.

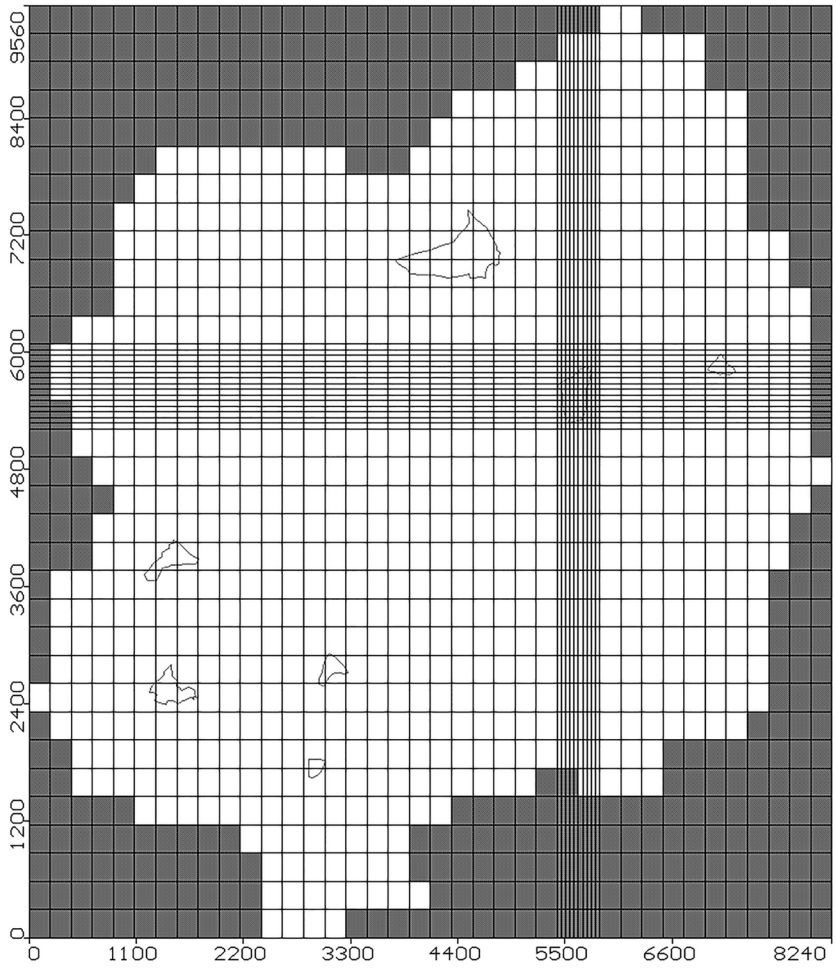

Figure 18.11 Discretized watershed with tanks.

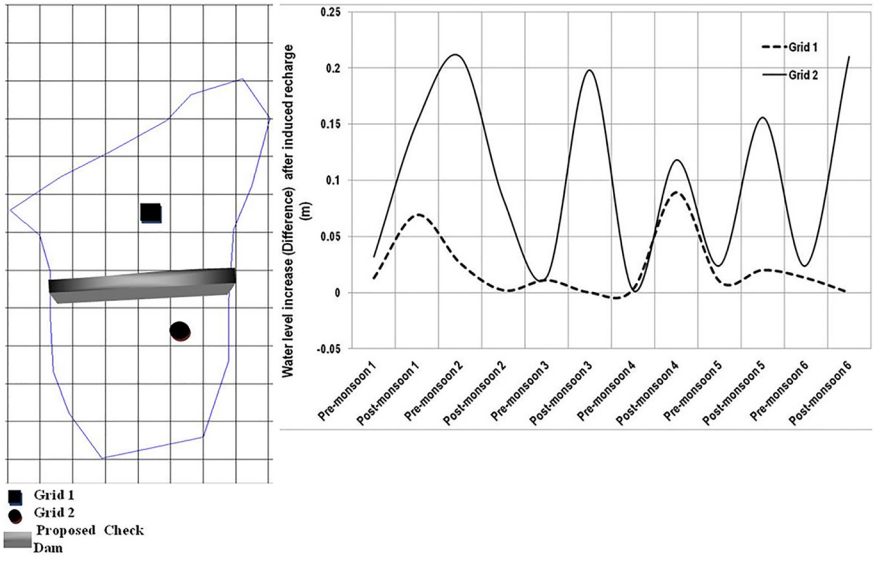

Figure 18.12 (a**)** Discretised Tumlur tank and (b) Impact of induced recharge on tank grid water level.

It is very clear that in spite of all other conditions being same, the space available in the northern part (that is lowest by natural way) was not enough for the artificial recharge to happen and the water would have been lost due to evaporation. The space available in the sub-surface has been comparatively more and hence with same amount of run-off water applied to the southern part using a check dam at an appropriate has provided more recharge to groundwater. This has been possible to acquire the prior knowledge using geophysical investigations.

18.5 CONCLUSIONS

The investigations documented above show that geophysical investigations along with geological knowledge provides insight to the sub-surface with considerable depth and have tremendous benefits for designing and performing MAR. MAR success could be badly affected in absence of such knowledge. In addition, we conclude that geophysical experiments have to be specially designed for MAR studies e.g., very close electrode spacing in case of VES as well as ERT and that application of TEM in alluvial formation etc. will enhance the applicability.

Artificial Recharge that is to enhance rainfall recharge by artificial means is a common and essential practice in MAR. The water available on the surface is put by a number of artificial means into the sub-surface and it is very important that the sub-surface and its characteristics are very well known. As MAR, check dams, dug wells and infiltration ponds are more prevalent, there is a need to understand the factors that control the movement of water in the unsaturated zone sub-surface beneath these ponds. Monitoring the hydrologic processes in the unsaturated zone is of great importance for improving MAR and geophysical instrumentation and monitoring is a potential method of identifying flow and transport processes in variably saturated media.

The geophysical information, to a great extent, provides knowledge and guidelines to determine the quantity and quality of the recharged water to the aquifer system and ensures both success and sustainability.

ACKNOWLEDGMENT

Authors are grateful to Director CSIR-NGRI, BRGM and the project team of Saph Pani. The work has been carried out with grant No. 281911 from the European Commission.

18.6 REFERENCES

Alexopoulos J. D., Dilalos S. and Vassilakis E. (2011). Adumbration of amvrakia's spring water pathways, based on detailed geophysical data(Kastraki – Meteora). *Advances in the Research of Aquatic Environment*, **2**, 105–122. doi:10.1007/978–3–642–24076-8.

Arora, T. and Shakeel A. (2010). Electrical structure of an unsaturated zone – a case study related to hard rock aquifer. *Current Science*, **99**(2), 216–220.

Arora T. and Ahmed S. (2011). Characterization of recharge through complex vadose zone of a granitic aquifer by time-lapse electrical resistivity tomography. *Journal of Applied Geophysics*, **73**, 35–44.

Arora T., Linde N., Revil A. and Castermant J. (2007). Non-intrusive characterization of the redox potential of landfill leachate plumes from self-potential data. *Journal of Contaminant Hydrology*, **92**, 274–292, doi:10.1016/j.jconhyd.2007.01.018.

Arora T. (2013). Hydrogeophysical characterization of unsaturated zone. Lambert Academic Publications, ISBN: 978–659–43870–7.

Binley A., Cassiani G., Middleton R. and Winship P. (2002). Vadose zone flow model parameterisation using cross-borehole radar and resistivity imaging. *Journal of Hydrology*, **267**(3–4), 147–159. doi:10.1016/S0022–1694.

Blizkovsky M. (1979). Processing and application in microgravity surveys. *Geophys. Prospect.*, **27**, 848–861.

Boisson A., Baisset M., Alazard M., Perrin J., Villesseche D., Dewandel B., Kloppmann W., Chandra S., Picot-Colbeaux G., Sarah S., Ahmed S. and Maréchal J. C. (2014). Comparison of surface and groundwater balance approaches in the evaluation of managed aquifer recharge structures: Case of a percolation tank in a crystalline aquifer in India, *Journal of Hydrology*, **519**, 1620–1633.

Bosch F. P. and Müller I. (2001). Continuous gradient VLF measurements: A new possibility for high resolution mapping of karst structures. *First Break*, **19**, 343–350.

Bosch F. P. and Müller I. (2005). Improved karst exploration by VLF-EM gradient survey: Comparison with other geophysical methods. *Near Surf Geophys*, **3**, 299–310.

Butler K. (1984). Microgravimetric and gravity gradient techniques for detection of subsurface cavities. *Geophysics*, **49**, 1084–1096.

Carriere S. D., Chalikakis K., Sénéchal G., Danquigny C.and Emblanch C. (2013) Combining electrical resistivity tomography and ground penetrating radar to study geological structuring of karst unsaturated zone. *J. Appl. Geophysm.,* **94**, 31–40.

China Geological Survey (CGS). (2005). Groundwater exploration in the arid and semiarid areas in China (Episode 2). Geological Publishing House, Beijing.

Chalikakis K. (2006). Application de méthodes géophysiques pour la reconnaissance et la protection des ressources en eau dans les milieux karstiques (Geophysical methods applied to water exploration and protection in karst environment). PhD Thesis, Université Pierre et Marie Curie, Paris, France.

Chen S. (1988). The use of selected frequency of natural field in finding water. *Site Investigation Science and Technology*, **2**, 53–55.

Colley G. C. (1963). The detection of caves by gravity measurements. *Geophys. Prospect.*, **11**, 1–9.

Dahlin T. and Zhou B. (2004). A numerical comparison of 2-D resistivity imaging with 10 electrode arrays. *Geophysical Prospecting*, **52**, 379–398.

DeGroot-Hedlin C. and Constable S. C. (1990). Occam's inversion to generate smooth, two dimensional models from magnetotelluric data. *Geophysics*, **55**, 1613–1624.

Dewandel B., Lachassagne P., Wyns R., Maréchal J. C. and Krishnamurthy N. S. (2006). A generalized 3-D geological and hydrogeological conceptual model of granite aquifers controlled by a single or multiple weathering. *J. Hydrol.*, **330**, 260–284.

Dey A. and Morrison H. F. (1979a). Resistivity modelling for arbitrary shaped two dimensional structures. *Geophysical Prospecting*, **27**(1), 106–136.

Dey A. and Morrison H. F. (1979b). Resistivity modelling for arbitrarily shaped three dimensional shaped structures. *Geophysics*, **44**(4), 753–780.

Dillon P. (2005). Future management of aquifer recharge. *Hydrogeol. J.*, **13**, 313–316.

Dillon P., Pavelic P., Page D., Beringen H. and Ward J. (2009). Managed aquifer recharge: An Introduction. Waterlines Report Series No. 13, National Water Commission, Canberra ACT 2600, Australia.

Dutta S., Krishnamurthy N. S., Arora T., Rao V. A. and Ahmed S. (2006). Localization of water bearing fractured zones in a hard rock area using integrated geophysical techniques in Andhra Pradesh, India. *Hydrogeology Journal*, **14**(5), 760–766.

Ezersky M., Bruner I., Keydar S., Trachtman P. and Rybakov M. (2006). Integrated study of the sinkhole development site on the western shores of the dead sea using geophysical methods. *Near Surf. Geophys.*, **4**, 335–343.

Farrell D., Mayers B. L., Moseley L., Sandberg S., Mwansa J., Sutherland A. and Barnes H. (2003). Geophysical imaging of seawater intrusion into karst limestones to support groundwater modelling along the west coast of Barbados [On-line]. Available: http://scitec.uwichill.edu.bb/OAS/Reports/Reports.htm

Gale I. and Dillon P. (2005). Strategies for Managed Aquifer Recharge (MAR) in semi-arid areas. United Nations Environment Programme, Division of Technology, Industry and Economics, UNESCO IHP, Paris, France.

Gan F. P., Yu L. P. and Lu C. J. (2011). Geophysical prospecting and analyzing on different karst waterbearing structures. *Geology and Exploration*, **47**(435), 663–672.

Gan F., Chen Y., Zhao W., Chen Y. and Liu W. (2013). Integrated geophysical methods for groundwater exploration in a karst area with or without thin cover – a case study from Tai'an City, Shandong Province, China. 13th Multidisciplinary Conference on Sinkholes and the Engineering and Environmental Impacts of Karst, Carlsbad, New Mexico, United States.

Ghosh D. P. (1971). The application of linear filter theory to the direct interpretation of geoelectrical resistivity sounding measurements. *Geophysical Prospecting*, **19**(2), 192–217.

Griffiths D. H., Turnbull J. and Olayinka A. I. (1990). Two dimensional resistivity mapping with a computer-controlled array. *First Break*, **8**(4), 121–129.

Guérin R., Baltassat J. M., Boucher M., Chalikakis K., Galibert P. Y., Girard J. F., Plagnes V. and Valois R. (2009). Geophysical characterisation of karstic networks – application to the ouysse system (Poumeyessen, France). *Applied Geophysics*, **341**, 810–817.

Jacob T., Chéry J., Bayer R., Le Moigne N., Boy J. P., Vernant P. and Boudin F. (2009). Time-lapse surface to depth gravity measurements on a karst system reveal the dominant role of the epikarst as a water storage entity. *Geophys. J. Int.*, **177**, 347–360. doi:10.1111/j.1365–246X.2009.04118.x

Jardani A., Revil A., Akoa F., Schmutz M., Florsch N. and Dupont J. P. (2006). Least squares inversion of self-potential (SP) data and application to the shallow flow of ground water in sinkholes. *Geophysical Research Letters*, **33**(19), L19306. doi:10.1029/2006GL027458.

Kaspar M. and Pecen J. (1975). Finding the caves in a karst formation by means of electromagnetic waves. *Geophys. Prospect.*, **23**, 611–621.

Koefoed O. (1979). Geosounding Principles 1: Resistivity Sounding Measurements. Elsevier Science Publishing Company, Amsterdam.

LaBrecque D. J. and Casale D. (2002). Experience with anisotropic inversion for electrical resistivity tomography: Proceedings of the Symposium on the Application of Geophysics to Engineering and Environmental Problems (SAGEEP) '02, compact disk paper 11ELE7.

Leucci G and De Giorgi L. (2005). Integrated geophysical surveys to assess the structural conditions of a karstic cave of archaeological importance. *Natural Hazards and Earth System Sciences*, **5**, 17–22.

Li G. Z. and Wang X. (2009). Application effect of water prospecting in granite region by comprehensive geophysical methods. *Site Investigation Science and Technology*, **4**, 55–57.

Li Y. and Oldenburg D. W. (1992). Approximate inverse mappings in DC resistivity problems. *Geophysical Journal International*, **109**(2), 343–362.

Loke M. H. and Barker R. D. (1996a). Rapid least-squares inversion of apparent resistivity pseudosections using a quasi-Newton method. *Geophysical Prospecting*, **44**(1), 131–152.

Loke M. H. and Barker R. D. (1996b). Practical techniques for 3D resistivity surveys and data inversion. *Geophysical Prospecting*, **44** (3), 499–523.

Loke M. H., Chambers J. E., Rucker, D. F., Kuras O. and Wilkinson P. B. (2013). Recent developments in the direct-current geoelectrical imaging method. *Journal of Applied Geophysics*, **95**, 135–156.

Loke M. H., Dahlin T. and Rucker D. F. (2014). Smoothness-constrained time-lapse inversion of data from 3-D resistivity surveys. *Near Surface Geophysics*, **12**(1), 5–24.

Metwaly M., Elawadi E. and Moustafal S. R. (2012). Groundwater exploration using geoelectrical resistivity technique at Al-Quwy'yia area central Saudi Arabia. *International Journal of Physical Sciences*, **7**(2), 317–326.

Meyerhoff S. B., Karaoulis M., Fiebig F., Maxwell R. M., Revil A., Martin J. B. and Graham W. D. (2012). Visualization of conduit-matrix conductivity differences in a karst aquifer using time-lapse electrical resistivity, *Geophysical Research Letters*, **39**(24), L24401. doi: 10.1029/2012GL053933.

Moore D. L. and Stewart M. T. (1983). Geophysical signatures of fracture traces in a karst aquifer (Florida, U.S.A.). *J. Hydrol.*, **61**, 325–340.

Neumann R. (1965). La gravimètrie de haute precision: Application aux recherches de cavités (high precision gravimetry: Application to cavities research). *Geophys. Prospect.*, **15**, 116–134.

Saydam A. S. and Duckworth K. (1978). Comparison of some electrode arrays for their IP and apparent resistivity responses over a sheet like target. *Geoexploration*, **16**(4), 267–289.

Singha, K., Day-Lewis, F. D., Johnson, T., and Slater, L. D. (2014). Advances in interpretation of subsurface processes with time-lapse electrical imaging. Hydrological Processes, DOI: 10.1002/hyp.10280.

Szalai S. and Szarka L. (2008). On the classification of surface geoelectric arrays. *Geophysical Prospecting*, **56**(2), 159–175.

Turberg P. and Barker R. (1996). Joint application of radio-magnetotelluric and electrical imaging surveys in complex subsurface environments. *First Break*, **14**, 105–112.

Vargemezis G., Tsourlos P. and Stampolidis A. (2012). A focusing approach to ground water detection by means of electrical and EM methods: The case of Paliouri, Northern Greece. *Studia Geophysica et Geodaetica*, **56**(4), 1063–1078.

Vlahović T. and Munda B. (2011). Karst aquifers on small islands—the island of Olib, Croatia. *Environ Monit Assess.*, **184**, 6211–6228.

Zaidi F. K. and Kassem O. M. K. (2012). Use of electrical resistivity tomography in delineating zones of groundwater potential in arid regions: A case study from Diriyah region of Saudi Arabia. *Arabian Journal of Geosciences*, **5**(2), 327–333.

Zhou W., Beck B. F. and Adams A. L. (2002). Effective electrode array in mapping karst hazards in electrical resistivity tomography. *Environmental Geology*, **42**(8), 922–928.